J. Plasma Physics (2003), *vol.* 69, *part* 4, *pp.* 305–330.
DOI: 10.1017/S0022377803002319 Printed in the United Kingdom

Nonlinear stationary whistler waves and whistler solitons (oscillitons). Exact solutions

E. DUBININ[1], K. SAUER[2] and J.F. McKENZIE[1,2]

[1]Max-Planck Institut fur Aeronomie, Katlenburg-Lindau, Germany
(dubinin@linmpi.mpg.de)

[2]School of Pure and Applied Physics, University of Natal, Durban, South Africa

(Received 4 November 2002 and in revised form 20 January 2003)

Abstract. A fully nonlinear theory for stationary whistler waves propagating parallel to the ambient magnetic field in a cold plasma has been developed. It is shown that in the wave frame proton dynamics must be included in a self-consistent manner. The complete system of nonlinear equations can be reduced to two coupled differential equations for the transverse electron or proton speed and its phase, and these possess a phase-portrait integral which provides the main features of the dynamics of the system. Exact analytical solutions are found in the approximation of 'small' (but nonlinear) amplitudes. A soliton-type solution with a core filled by smaller-scale oscillations (called 'oscillitons') is found. The dependence of the soliton amplitude on the Alfvén Mach number, and the critical soliton strength above which smooth soliton solutions cannot be constructed is also found. Another interesting class of solutions consisting of a sequence of wave packets exists and is invoked to explain observations of coherent wave emissions (e.g. 'lion roars') in space plasmas. Oscillitons and periodic wave packets propagating obliquely to the magnetic field also exist although in this case the system becomes much more complicated, being described by four coupled differential equations for the amplitudes and phases of the transverse motion of the electrons and protons.

1. Introduction

Whistlers are right-handed polarized electromagnetic waves which propagate at frequencies less than the electron gyrofrequency in a magnetized plasma. The dispersion relation for these waves propagating parallel to the magnetic field in a cold plasma is (Stix 1992)

$$\frac{k^2}{\omega^2} = \frac{1}{c^2} + \frac{1}{V_{\mathrm{Ap}}^2(1+\omega/\Omega_{\mathrm{p}})} + \frac{1}{V_{\mathrm{Ae}}^2(1-\omega/\Omega_{\mathrm{e}})}, \tag{1a}$$

in which the electrons and protons appear on an equal footing, $V_{\mathrm{Ap,e}}$ is the Alfvén speed based on the proton (electron) mass density and $\Omega_{\mathrm{p,e}}$ are the gyrofrequencies. The classical Appleton–Hartle form of magneto-ionic theory follows from the high frequency ($\omega \gg \Omega_{\mathrm{p}}$) approximation which gives the refractive index ($n = ck/\omega$) as

$$n^2 = 1 + \frac{\omega_{\mathrm{pe}}^2}{\omega(\Omega_{\mathrm{e}} - \omega)}, \tag{1b}$$

in which we have used $V_{\rm Ap}^2/\Omega_{\rm p} = V_{\rm Ae}^2/\Omega_{\rm e}$ and the identity $V_{\rm Ae}^2/\Omega_{\rm e}^2 = c^2/\omega_{\rm pe}^2$, where $\omega_{\rm pe}$ is the electron plasma frequency. In this massive proton approximation ($m_{\rm p} \to \infty$) the proton mass disappears implying that the protons simply provide a quasineutralizing background to the electron motion. However, in the nonlinear treatment, as will be shown subsequently, the inclusion of the proton dynamics is crucial to the formation of nonlinear waves associated with the whistler mode. Furthermore, if $V_{\rm Ae}^2 \ll c^2$ (or $\omega_{\rm pe} \gg \Omega_{\rm e}$) (1b) approximates to

$$\frac{k^2}{\omega^2} = \frac{1}{V_{\rm Ae}^2}\left(\frac{\Omega_{\rm e}^2}{\omega(\Omega_{\rm e}-\omega)}\right) \tag{1c}$$

which form implies that for wave speeds much less than c we may neglect the displacement current in Maxwell's equations. Formally this is equivalent to the limit $\epsilon_0 \to 0$ ($c \to \infty$) so that Poisson's equation requires quasineutrality. For whistlers, $\omega \leqslant \Omega_{\rm e}$, this is a very good approximation in many space plasmas, such as the magnetosphere and solar wind, and we shall use it in the subsequent nonlinear treatment which is thereby simplified through the neglect of the electric stresses (i.e. $\epsilon_0 E_x^2/2, \epsilon_0 E_x E_{y,z}$) in the momentum conservation equations (10)–(12) given below.

An especially interesting feature of whistler waves is the existence of a maximum of the phase speed ω/k (at $\omega/k = V_{\rm Ae}/2$ for waves propagating parallel to the magnetic field at $\Omega_{\rm e}/2$) where the phase and group velocities are equal. A similar feature, i.e. the appearance of points, maxima or minima in the ω/k–k space, arises in the dispersion properties of low-frequency waves in multi-ion plasmas. It has been shown (Sauer et al. 2001, 2002a; Dubinin et al. 2002) that such a system admits the existence of a new class of stationary nonlinear solutions, called 'oscillitons', characterized by spatial oscillations which are superimposed on the soliton-like pulses. Sauer et al. (2002b) recently also pointed out that whistler oscillitons arise from the existence of a maximum in the phase speed. The concept of oscillitons was invoked to explain the observation of coherent wave emissions observed in the Earth's magnetosheath and polar cusp, known as 'lion roars'.

In these papers (Sauer et al. 2001, 2002a; Dubinin et al. 2002) oscilliton structures were found by numerically integrating the full set of completely nonlinear equations describing the system, leaving open the questions of whether oscillitons are a new class of soliton-like solutions or periodic nonlinear stationary waves, and what is the strength of an oscilliton as a function of its Mach number, and its critical amplitude (or Mach number) (if it does exist). In this paper we address these questions by investigating (analytically) nonlinear stationary whistlers and solitons propagating parallel and obliquely to the magnetic field in a cold plasma. It is found that oscillitons are indeed a new specific class of soliton structures. Note that soliton solutions were also considered by Montgomery (1959) and Kakutani (1966) in terms of a pseudo-particle motion in Sagdeev's potential.

The layout is organized as follows. The governing equations, given in Sec. 2, are the standard equations of motion for the electrons and protons and the Maxwell equations. The linear dispersion equation for stationary waves of the form $f(x+Ut)$ propagating with speed U provides us with the necessary condition for the existence of soliton structures. In contrast to classical evanescent types of solutions, with imaginary wave number, the wave number for stationary whistlers is complex, i.e. the structures are characterized by spatial oscillations which are superposed on

https://doi.org/10.1017/S0022377803002319 Published online by Cambridge University Press

the spatial growth or decay. Another important conclusion which follows already from the linear treatment is that in the wave frame the transverse momentum carried by the electrons and protons is of the same order and therefore the proton dynamics is essential in the nonlinear analysis. The full system of completely nonlinear equations describing whistlers propagating parallel to the magnetic field is given in Sec. 3 with the proton dynamics included in a self-consistent manner. The neglect of the proton contribution only leads to trivial solutions.

In addition to the standard integrals of motion (momentum and energy fluxes) we find a new constant of the motion which allows us to reduce the full system of differential equations to two coupled differential equations for the transverse amplitude and its phase ϕ. In Secs 3.1 and 3.2 we consider the approximations of small (and arbitrary) phases and small (but nonlinear) amplitudes, and analyse phase portraits of the system. At electron Alfvén Mach numbers $M_{\rm Ae}$ in excess of the threshold value ($M_{\rm Ae} = 1/2$) there is a family of periodic orbits around an O-type point limited by a heteroclinic orbit connecting two saddle points. The latter trajectory corresponds to a soliton-type solution. In contrast to classical solitons, whistler solitons contain an oscillatory part, and hence are called oscillitons. Exact expressions for the amplitude and phases are found. The strength of oscillitons is determined by the Mach number and it is shown that already at the Mach number $M_{\rm Acrit} = 1/\sqrt{2} \approx 0.7$, smooth oscillitons cannot be constructed. Another interesting class of solutions also exists at $M_{\rm Ae} = 1/2$, consisting of a sequence of wave packets. The amplitude of these waves is determined by the initial perturbation of the system. In Sec. 4 we discuss stationary waves propagating obliquely to the magnetic field. Although in this case the system is described by four coupled differential equations, the main features of stationary solutions can, nevertheless, be elucidated in certain approximations.

2. Governing equations and the dispersion relation of stationary waves

In a cold magnetized plasma consisting of protons (p) and electrons (e) the fluid equations for each constituent are

$$\frac{\partial n_{\rm p,e}}{\partial t} + \nabla \cdot (n_{\rm p,e}\mathbf{u}_{\rm p,e}) = 0, \tag{2}$$

$$m_{\rm p,e} n_{\rm p,e} \frac{D_{\rm p,e}\mathbf{u}_{\rm p,e}}{Dt} = e n_{\rm p,e} q_{\rm p,e}(\mathbf{E} + \mathbf{u}_{\rm p,e} \times \mathbf{B}), \tag{3}$$

where $m_{\rm p,e}$ is the mass (p, protons, e, electrons), $q_{\rm p,e} = \pm 1$ the charge, $n_{\rm p,e}$ the number density and $u_{\rm p,e}$ the velocity, whilst $\mathbf{B}$ and $\mathbf{E}$ are the magnetic and electric fields, respectively, and the convective derivative is

$$\frac{D_{\rm p,e}}{Dt} = \frac{\partial}{\partial t} + \mathbf{u}_{\rm p,e} \cdot \nabla. \tag{4}$$

The remaining equations are Faraday's and Ampere's laws

$$\frac{\partial \mathbf{B}}{\partial t} = -\mathrm{curl}\, \mathbf{E}, \tag{5}$$

$$\mathrm{curl}\, \mathbf{B} = \mu_0 \mathbf{j}, \tag{6}$$

https://doi.org/10.1017/S0022377803002319 Published online by Cambridge University Press

in the latter of which we neglect the displacement current, and the current $\mathbf{j}$ is given by

$$\mathbf{j} = e(n_{\mathrm{p}}\mathbf{u}_{\mathrm{p}} - n_{\mathrm{e}}\mathbf{u}_{\mathrm{e}}). \tag{7}$$

This is the standard fluid description in which electron inertia is not neglected and the proton dynamics is also included, that is to say both are placed on an equal footing. Our subsequent analysis of stationary, nonlinear whistler waves shows that the latter, the inclusion of proton dynamics, is crucial for the correct description of nonlinear waves in the wave frame.

We first consider the simplest case of stationary waves of the form $f(x + Ut)$ propagating parallel to the magnetic field ($\mathbf{B} = (B, 0, 0)$). It is convenient to carry out the formulation and analysis in the wave frame so that the plasma appears to be flowing with speed $u_{\mathrm{p}} = u_{\mathrm{e}} = u_0 = (+U)$ along the x-axis. The system has the following integrals of motion. The number flux of each species is constant,

$$n_{\mathrm{p,e}} u_{\mathrm{p}x,\mathrm{e}x} = f_{\mathrm{p,e}} = \text{const}. \tag{8}$$

The quasineutrality assumption $n_{\mathrm{p}} = n_{\mathrm{e}}$ (which is valid if $\omega_{\mathrm{pe}} \gg \Omega_{\mathrm{e}}$) combined with zero current in the x-direction, $j_x = 0$, yields $u_{\mathrm{p}x} = u_{\mathrm{e}x}$. Faraday's law implies that $E_y = \text{const}$ and $E_z = \text{const}$ so that for motion parallel to the magnetic field

$$E_y = 0, \quad E_z = 0. \tag{9}$$

Total momentum conservation requires

$$\sum_{\mathrm{p,e}} m_{\mathrm{p,e}} f_{\mathrm{p,e}} u_{\mathrm{p}x,\mathrm{e}x} + \frac{B_y^2 + B_z^2}{2\mu_0} = \text{const}, \tag{10}$$

$$\sum_{\mathrm{p,e}} m_{\mathrm{p,e}} f_{\mathrm{p,e}} u_{\mathrm{p}y,\mathrm{e}y} - \frac{B_x B_y}{\mu_0} = \text{const}, \tag{11}$$

$$\sum_{\mathrm{p,e}} m_{\mathrm{p,e}} f_{\mathrm{p,e}} u_{\mathrm{p}z,\mathrm{e}z} - \frac{B_x B_z}{\mu_0} = \text{const}, \tag{12}$$

in which the electric stresses are neglected in this quasineutral approximation. Total energy flux conservation is simply

$$\sum_{\mathrm{p,e}} f_{\mathrm{p,e}} \frac{m_{\mathrm{p,e}}\left(u_{\mathrm{p}x,\mathrm{e}x}^2 + u_{\mathrm{p}y,\mathrm{e}y}^2 + u_{\mathrm{p}z,\mathrm{e}z}^2\right)}{2} = \text{const} \tag{13}$$

(because the Poynting flux $(\mathbf{E} \times \mathbf{B})_x/\mu_0$ is zero). Assuming that at $x = -\infty, n_{\mathrm{p}} = n_{\mathrm{e}} = 1, u_{\mathrm{p}x,\mathrm{e}x} = u_0 = 1$, and $B = B_x = B_0 = 1$, the normalized conservation equations become

$$n_{\mathrm{p}} u_{\mathrm{p}x} = f_{\mathrm{p}} = 1, n_{\mathrm{e}} u_{\mathrm{e}x} = f_{\mathrm{e}} = 1, \tag{14}$$

$$\mu(u_{\mathrm{p}x} - 1) + (u_{\mathrm{e}x} - 1) + \frac{1}{2M_{\mathrm{A}}^2}\left(B_y^2 + B_z^2\right) = 0, \tag{15}$$

$$\mu u_{\mathrm{p}y} + u_{\mathrm{e}y} = B_y/M_{\mathrm{A}}^2, \tag{16}$$

$$\mu u_{\mathrm{p}z} + u_{\mathrm{e}z} = B_z/M_{\mathrm{A}}^2, \tag{17}$$

$$\mu\left(u_{\mathrm{p}x}^2 - 1\right) + \left(u_{\mathrm{e}x}^2 - 1\right) + \mu\left(u_{\mathrm{p}y}^2 + u_{\mathrm{p}z}^2\right) + \left(u_{\mathrm{e}y}^2 + u_{\mathrm{e}z}^2\right) = 0, \tag{18}$$

https://doi.org/10.1017/S0022377803002319 Published online by Cambridge University Press

where $\mu = m_{\rm p}/m_{\rm e}$ and $M_{\rm A}$ is the electron Alfvén Mach number of the plasma flow at $x = -\infty$, $M_{\rm A}^2 = u_0^2/V_{\rm Ae}^2$ ($V_{\rm Ae} = B_0/\sqrt{\mu_0 n_{\rm e0} m_{\rm e}}$ is the Alfvén speed based on the electron mass density), and we write $u_{{\rm p}x} = u_{{\rm e}x} = u_x$ by virtue of the quasi-charge neutral approximation.

Using these equations, B_y, B_z and u_x may be expressed as functions of the transverse velocity components of the protons and electrons. The remaining equations, which close the system, are the differential equations of motion for the transverse velocities $u_{{\rm p}y}, u_{{\rm p}z}, u_{{\rm e}y}$ and $u_{{\rm e}z}$, namely

$$\mu u_x \frac{du_{{\rm p}y}}{dx} = u_{{\rm p}z} - u_{{\rm p}x} B_z, \tag{19a}$$

$$\mu u_x \frac{du_{{\rm p}z}}{dx} = u_{{\rm p}x} B_y - u_{{\rm p}y}, \tag{19b}$$

$$u_x \frac{du_{{\rm e}y}}{dx} = -(u_{{\rm e}z} - u_{{\rm e}x} B_z), \tag{20a}$$

$$u_x \frac{du_{{\rm e}z}}{dx} = -(u_{{\rm e}x} B_y - u_{{\rm e}y}). \tag{20b}$$

Here the spatial variable x is normalized to $u_0/\Omega_{\rm e}$, where $\Omega_{\rm e} = eB_0/m_{\rm e}$ is the electron gyrofrequency, and is therefore an electron gyroradius based on the wave speed.

Before analysing nonlinear waves we briefly discuss the linearized equations and derive the dispersion equation for stationary waves. Using the complex variables $u_{{\rm e}\pm} = u_{{\rm e}y} \pm i u_{{\rm e}z}, u_{{\rm p}\pm} = u_{{\rm p}y} \pm i u_{{\rm p}z}, B_\pm = B_y \pm i B_z$, the linearized equations (19) and (20) become

$$\frac{du_{{\rm e}\pm}}{dx} = \mp i\big[M_{\rm A}^2(u_{{\rm e}\pm} + \mu u_{{\rm p}\pm}) - u_{{\rm e}\pm}\big], \tag{21a}$$

$$\mu \frac{du_{{\rm p}\pm}}{dx} = \pm i\big[M_{\rm A}^2(u_{{\rm e}\pm} + \mu u_{{\rm p}\pm}) - u_{{\rm p}\pm}\big]. \tag{21b}$$

Seeking solutions of the form $u_{{\rm e}+} = u_{{\rm e}+} e^{ikx}$, $u_{{\rm p}+} = u_{{\rm p}+} e^{ikx}$, (21) yields the dispersion equation

$$k^2 - k + M_{\rm A}^2 = 0, \tag{22}$$

(in which we have used the fact that $\mu - 1 \cong \mu$) with the roots

$$k_{1,2} = \frac{1 \pm \sqrt{1 - 4M_{\rm A}^2}}{2}, \tag{23}$$

which agrees with the stationary wave form of (1c) in which we put $\omega = kU$ and $M_{\rm A} = U/V_{\rm Ae}$. It follows that periodic solutions exist for $M_{\rm A} < 1/2$. However, for $M_{\rm A} > 1/2$, k is complex and stationary structures are characterized by spatial oscillations which are superimposed on the spatial growth or decay. The real part of k gives the wave number of the oscillations and the imaginary part determines the spatial growth of the amplitude. With $M_{\rm A}^2 = 1/4(1+\delta)^2$, (23) may be written as

$$k_r = 1/2, \quad k_i = \sqrt{\delta/2}\,. \tag{24}$$

Since the expression for k does not contain the proton mass it would be tempting to draw the conclusion that proton dynamics may be neglected (in agreement with

the classical dispersion analysis for whistlers). However, as we already mentioned and as will be shown subsequently, the momentum exchange between the protons and electrons becomes vitally important in nonlinear structures. It is useful to note even in this linearized version that in the wave frame the ratio of the transverse speeds of the electrons and protons $u_{e\pm}/u_{p\pm} \sim O(\mu)$ as, indeed, (21) shows,

$$\frac{u_{e\pm}}{u_{p\pm}} = -\frac{\mu}{1 + (\kappa/M_A^2) - (1/M_A^2)} \tag{25a}$$

or

$$\frac{u_{e+}}{u_{p+}} = \frac{u_{e-}}{u_{p-}} \approx \mu[(1-6\delta) \pm i\sqrt{8\delta}\,] \quad (\delta \ll 1). \tag{25b}$$

This clearly demonstrates that the transverse momentum fluxes as carried by the protons and the electrons are of the same order.

3. Nonlinear stationary whistlers propagating parallel to the magnetic field

The fully nonlinear equations for the transverse velocities of the electrons and protons in complex form are

$$\frac{du_{e\pm}}{dx} = \mp i\big[M_A^2(u_{e\pm} + \mu u_{p\pm}) - u_{e\pm}/u_x\big], \tag{26a}$$

$$\mu\frac{du_{p\pm}}{dx} = \pm i\big[M_A^2(u_{e\pm} + \mu u_{p\pm}) - u_{p\pm}/u_x\big]. \tag{26b}$$

Multiplying (26a) by $u_{e\mp}$ and adding yields

$$\frac{d|u_e|^2}{dx} = iM_A^2\mu(u_{e+}u_{p-} - u_{e-}u_{p+}). \tag{27a}$$

Similarly,

$$\mu\frac{d|u_p|^2}{dx} = iM_A^2(u_{e+}u_{p-} - u_{e-}u_{p+}), \tag{27b}$$

where $|u_e|^2 = u_{e+}\cdot u_{e-}$ and $|u_p|^2 = u_{p+}\cdot u_{p-}$. Hence

$$\frac{d|u_e|^2}{\mu d|u_p|^2} = \mu \quad \text{or} \quad |u_e|^2 = \mu^2|u_p|^2. \tag{28}$$

Then, using the ansatz $u_{p\pm} = |u_p|e^{\pm i\phi_p}$, $u_{e\pm} = |u_e|e^{\pm i\phi_e}$, (27a) can be written in the form

$$\frac{du_e}{dx} = M_A^2 u_e \sin\phi, \tag{29}$$

where $\phi = \phi_p - \phi_e$. It can be readily shown that $d|u_e|/dx = 0$ if we neglect the proton contribution in (26a), and therefore the most important class of solutions in which $|u_e| \neq$ const would be lost. Moreover, even if we were to include the proton dynamics only in the massive proton approximation, it also follows from the linearized equation (25b) that $u_{e+}/u_{p+} = u_{e-}/u_{p-} \sim \exp(i\phi_0)$, with the result that the cross product $u_{e+}u_{p-} - u_{e-}u_{p+} = 0$, so that the phase $\phi = 0$ and again we would come to $|u_e| =$ const. These arguments show that the proton dynamics must be included in a self-consistent manner to describe the intricate structure of nonlinear waves.

https://doi.org/10.1017/S0022377803002319 Published online by Cambridge University Press

The differential equation for the phase ϕ follows from (26a) and (26b) in the form

$$\frac{d\phi}{dx} = 2M_A^2(\cos\phi + 1) - \frac{1}{\sqrt{1 - (u_e^2/\mu)}} \tag{30}$$

in which we have used $u_{e,p\pm} = |u_{e,p}|e^{\pm i\phi_{e,p}}$, $u_p = u_e/\mu$ and the energy flux relation (18) to express u_x in terms of u_e, i.e.

$$u_x = \sqrt{1 - \frac{\mu u_p^2 + u_e^2}{\mu + 1}} \approx \sqrt{1 - \frac{u_e^2}{\mu}}. \tag{31}$$

Equations (29) and (30) completely describe the structure of nonlinear stationary waves propagating in the whistler mode parallel to the magnetic field in a cold plasma.

In analysing these equations we first note that the system has equilibrium (fixed) points. One set of fixed points is at $u_e = 0$ and $\cos\phi = 1/2M_A^2 - 1$. The second set corresponds to $\sin\phi = 0$ and $u_e = \sqrt{\mu}\sqrt{1 - 1/16M_A^4}$. The system possesses an integral which provides us with an algebraic expression between u_e and $\cos\phi$. To this end note that (29) and (30) yield

$$\sin\phi\frac{d\phi}{du_e} = \frac{2M_A^2(\cos\phi + 1) - (1 - u_e^2/\mu)^{-1/2}}{M_A^2 u_e} \tag{32}$$

which, on using the integrating factor u_e^2, integrates immediately to give

$$\cos\phi = \frac{C}{u_e^2} - \frac{1}{M_A^2}\frac{\sqrt{1 - u_e^2/\mu}}{u_e^2/\mu} - 1, \tag{33}$$

where C is the integration constant. Alternatively (29) and (30) possess the integral

$$\Phi = u_e^2(\cos\phi + 1) + \frac{\sqrt{1 - u_e^2/\mu}}{M_A^2 u_e^2/\mu} \tag{34}$$

which shows that

$$\frac{d\Phi}{dt} = \frac{\partial\Phi}{\partial u}\frac{du}{dt} + \frac{\partial\Phi}{\partial\psi}\frac{d\psi}{dt} = 0, \tag{35}$$

and we have $\Phi = \text{const} = C$ along the solution trajectories. Thus with $\sin\phi$ as a function of u_e given by (33), (29) is a first-order differential equation for the spatial structure of u_e which admits soliton and periodic type solutions. In the following we consider in more detail different approximations to (29) and (30).

3.1. Approximation of small phases and amplitudes

With $M_A^2 = 1/4(1 + \delta)^2$, and assuming $\delta \ll 1$, one of the fixed points is at $u = 0, \phi \approx \pm\sqrt{8\delta}$. The second fixed point is at $\sin\phi = 0$ and $u_e = 2\sqrt{\mu\delta}$. Therefore the approximations $u_e^2 \ll \mu$ and small phases ($\phi \ll 1$) are valid for all but the largest amplitudes $u_e \sim \sqrt{\mu}$ and the structure equations (29) and (30) may be written in rescaled form,

$$\frac{du}{dt} = u\psi, \tag{36a}$$

$$\frac{d\psi}{dt} = 2\delta - \psi^2 - u^2, \tag{36b}$$

https://doi.org/10.1017/S0022377803002319 Published online by Cambridge University Press

in which $u^2 = u_e^2/2\mu$, $\psi = M_A\phi$ and $t = xM_A$. The system has two fixed points, one of which is a saddle or X-type ($u = 0, \psi = \pm\sqrt{2\delta}$) and the other one is a circle or O-type ($u = \sqrt{2\delta}\,, \psi = 0$) which in the original coordinates correspond to ($u_e = 0, \phi = \pm\sqrt{2\delta}/M_A$) and ($u_e = 2\sqrt{\delta\mu}\,, \phi = 0$), respectively.

Equations (36a) and (36b) possess the phase portrait integral

$$\Psi = \frac{u^2}{2}\left(2\delta - \psi^2 - \frac{u^2}{2}\right) \tag{37}$$

so that

$$\psi = \pm\sqrt{2\delta - u^2/2 - 2C_1/u^2}\,, \tag{38a}$$

$$\frac{du}{dt} = \pm u\sqrt{2\delta - u^2/2 - 2C_1/u^2}\,, \tag{38b}$$

where C_1 is a constant. Figure 1(a) shows the phase portrait (ψ, u) of the system. There is a family of periodic orbits around the fixed point ($u_e = 2\sqrt{\delta\mu}\,, \phi = 0$) limited by a heteroclinic orbit connecting two saddle points ($u_e = 0, \phi = \pm\sqrt{2\delta}/M_A$). The system is completely integrable and the solution can be reduced to the elliptic integral of the first kind

$$\int \frac{du}{\sqrt{2\delta u^2 - u^4/2 - 2C_1}} = \pm t, \tag{39a}$$

or

$$F(u, K) = \mp\sqrt{\frac{2\delta C_1^2}{\delta^2 - C_1}}\,t, \tag{39b}$$

where $F(u, K)$ is the elliptic integral of the first kind, and

$$K^2 = \frac{(1 - \sqrt{1 - (C_1/\delta^2)}\,)}{(1 + \sqrt{1 - (C_1/\delta^2)}\,)}. \tag{39c}$$

Then the amplitude u is

$$u = \mp\mathrm{sn}\left(\sqrt{\frac{2\delta C_1^2}{\delta^2 - C_1}}\,t, K\right), \tag{40}$$

where $\mathrm{sn}(t, K)$ is the Jacobi function.

The differential equation for the phase ψ which determines the characteristic wave number of the stationary waves takes the form

$$\frac{d\psi}{dt} = \pm\sqrt{(\psi^2 - 2\delta)^2 - 4C_1}\,. \tag{41}$$

However, these waves also contain smaller-scale oscillations whose wavelengths are determined by the phases ϕ_e (for the electrons) and ϕ_p (for the protons). For example, the wave number characterizing the small-scale oscillating part in the electron motion, embedded in the main structure, can be readily found as

$$\frac{d\phi_e}{dx} = 1/2 + 3u_e^2/8\mu - 2\mu C_1/u_e^2. \tag{42}$$

Consider first the most interesting solutions corresponding to the orbit connecting two saddle points. Positive (negative) values of the constant C_1 yield closed periodic

https://doi.org/10.1017/S0022377803002319 Published online by Cambridge University Press

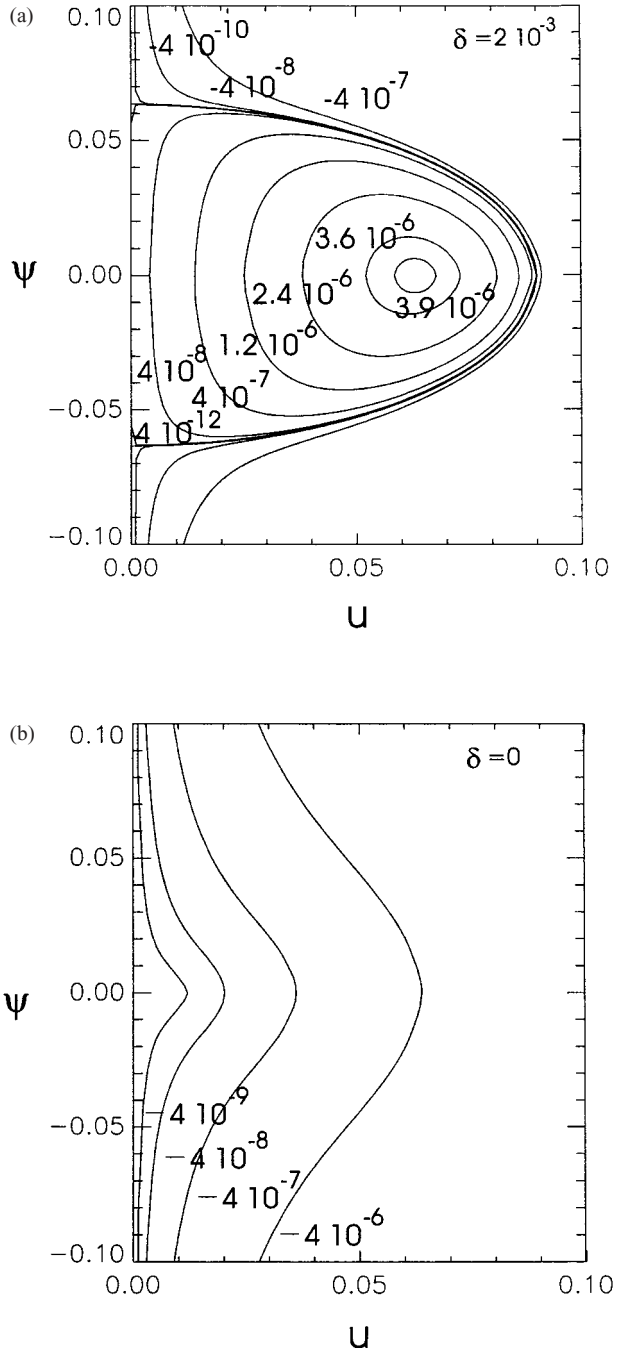

Figure 1. (a) The phase portrait of the system at $\delta = 2 \times 10^{-3}$. There is a family of periodic solutions (positive values of a constant C_1) around a circle point at $u = (2\delta)^{1/2}, \psi = 0$ limited by a heteroclinic trajectory (the bold curve) connecting two saddle points at $u = 0, \psi = \pm(2\delta)^{1/2}$. (b) The phase portrait of the system at $\delta = 0$. Two saddle points merge to one at $\psi = 0$. Trajectories at $C_1 < 0$ correspond to nonlinear stationary waves, the amplitude and period of which are determined by an 'initial perturbation'.

https://doi.org/10.1017/S0022377803002319 Published online by Cambridge University Press

(free) orbits (Fig. 1(a)). On the heteroclinic orbit, $C_1 = 0$ (the bold curve in Fig. 1(a)), which immediately gives the maximum amplitude of the structure $u_{\max} = 2\sqrt{\delta}$ (or $u_{\mathrm{emax}} = 2\sqrt{2\mu\delta}$). Integration of (38b) with $C_1 = 0$ ($u \neq 0$) yields a soliton-like solution,

$$\ln \frac{2\sqrt{\delta} + \sqrt{4\delta - u^2}}{u} = \mp\sqrt{2\delta}\, t, \tag{43}$$

or

$$u = \frac{4\sqrt{\delta}\exp(\pm\sqrt{2\delta}\, t)}{1 + \exp(\pm 2\sqrt{2\delta}\, t)}. \tag{44}$$

The width T (or $X = T/M_{\mathrm{A}}$) of the structure (at $u = u_{\max}/2$) is readily determined from (43),

$$T = \frac{2}{\sqrt{2\delta}} \ln(2 + \sqrt{3}), \tag{45}$$

i.e. it is similar to that of the classical soliton, namely the product of the amplitude and the width is a constant, in this case $2^{3/2}\ln(2+\sqrt{3})$. The significant difference is the presence of the smaller-scale oscillations related to the phases ϕ_{e} and ϕ_{p}. Figure 2(b) (the solid curve) shows u as a function of t for $\delta = 0.002$ ($M_{\mathrm{A}} = 0.501$). The dashed curve depicts the phase ψ. It varies from $\sqrt{2\delta}$ at $-\infty$ to $-\sqrt{2\delta}$ at $+\infty$, which corresponds to the infinite length of the motion along the heteroclinic (soliton) trajectory. An oscillating part embedded in the soliton structure is described by the value $d\psi_{\mathrm{e}}/dt$ (for the electrons) which varies according to

$$\frac{d\psi_{\mathrm{e}}}{dt} = 1/2 + 3/4u^2. \tag{46}$$

Integrating this equation, on using the expression (44), yields the phase $\psi_{\mathrm{e}} = \phi M_{\mathrm{A}}$ in the form

$$\psi_{\mathrm{e}} = 0.5t \mp 6\sqrt{\delta/2}\frac{1}{1 + \exp(\mp 2\sqrt{2\delta}\, t)} + \mathrm{const}, \tag{47}$$

where a constant of integration is determined from the merging of the solutions for $t < 0$ and $t > 0$. Figure 2(c) shows $d\phi_{\mathrm{e}}/dt$ as a function of t. The phase ϕ_{e} varies almost linearly with t undergoing only a small drift with amplitude within the core of the soliton. Figure 2(d) presents $u_y = u\cos(\psi_{\mathrm{e}})$ and $u_z = u\sin(\psi_{\mathrm{e}})$. The oscilliton structure exhibiting spatial oscillations, superimposed on the soliton profile, is clearly depicted.

Figure 3 presents the results for an oscilliton propagating at a slightly higher speed $M_{\mathrm{A}} = 0.51$ ($\delta = 0.02$). The amplitude (width) increases (decreases) according to (44) and (45). Correspondingly, the number of embedded oscillations decreases. The value $d\phi_{\mathrm{e}}/dt$ (=1/2 at $t \to \pm\infty$) drifts within the main structure reaching 0.55 at the centre of the soliton. For comparison, Fig. 4 shows the results of numerically solving the exact nonlinear equations (19) and (20) for oscillitons propagating with speeds $M_{\mathrm{A}} = 0.501$ and $M_{\mathrm{A}} = 0.51$. The good agreement justifies the approximation used. (To rescale the parameters to the original coordinates we make the transformation $u_{\mathrm{e}} = u\sqrt{2\mu}$, $x = t/M_{\mathrm{A}}$ and $\phi_{\mathrm{e}} = \psi_{\mathrm{e}}/M_{\mathrm{A}}$.)

It is interesting to note that at $\delta = 0$ ($M_{\mathrm{A}} = 1/2$) two saddle points degenerate into one at $\psi = 0$, and the phase portrait of the system reconfigures to that shown in Fig. 1(b). Soliton-like structures disappear but nonlinear stationary waves with different amplitudes remain. For the exact pair of differential equations (29) and (30) the saddle points appear periodically at $\psi = \pm n\pi$. Therefore one can expect

https://doi.org/10.1017/S0022377803002319 Published online by Cambridge University Press

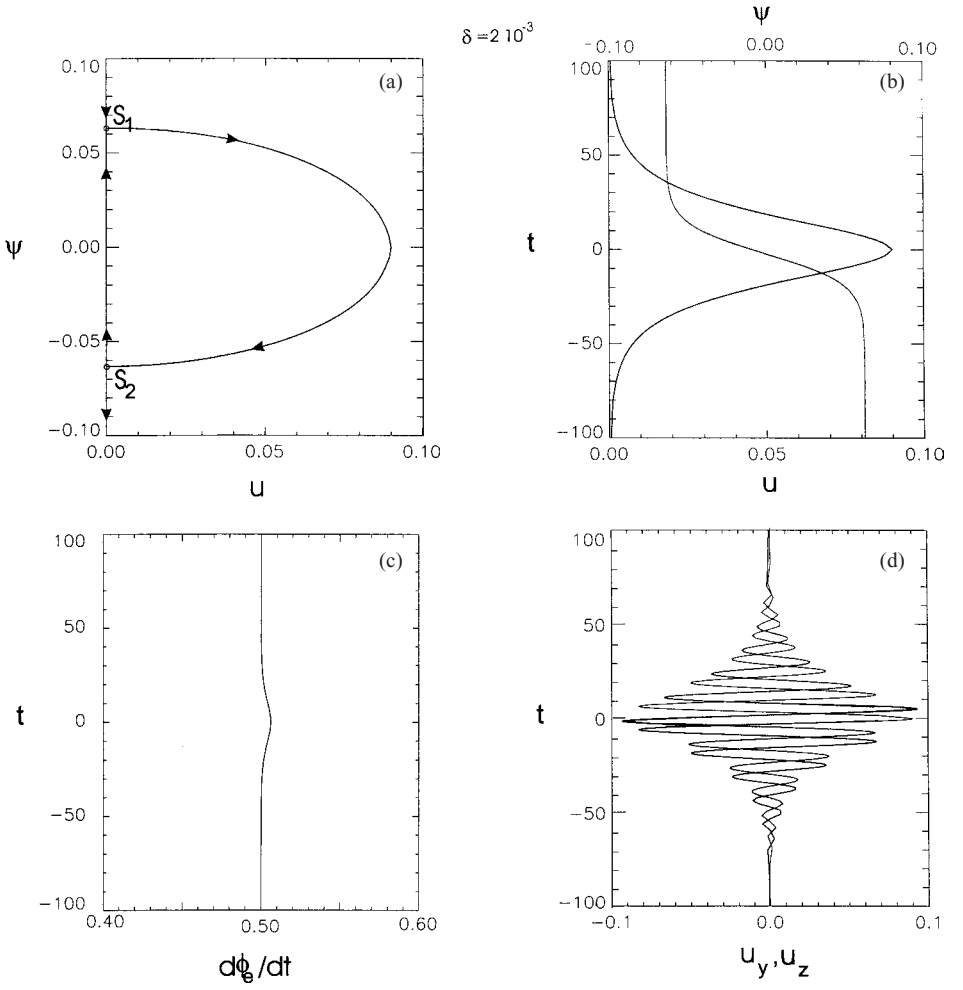

Figure 2. (a) The orbit connecting two saddle points S_1, S_2 corresponding to the soliton solution. (b) The envelope of oscilliton u as a function of distance t. The dashed curve shows the phase ψ which characterizes the width of the envelope. (c) The oscillating part of the electron motion is determined by the phase ψ_e. (d) The oscillating content embedded to the soliton (u_y and u_z are shown by the solid and dashed curves, respectively).

the existence of periodic nonlinear waves, the amplitude of which is a function of a constant C_1, $u = (4C_1)^{1/4}$ ('initial perturbation'). In common with oscillitons these waves contain smaller-scale oscillations so that the overall picture is one of a sequence of periodical wave packets. The width of the wave packets is determined by (41) with $\delta = 0$, and therefore it is also a function of the integration constant C_1. As C_1 increases the width of the wave packets $\Delta \approx 1/2(4C_1)^{-1/4}$ decreases. Small-scale oscillations have a wavelength determined by the expression (42) which is about $2\pi/0.5 = 4\pi$. Figure 5 shows an example of numerical integration of (19) and (20) for $M_A = 1/2$ and different 'initial disturbances' of the value u_{ey}. It will be observed that the system 'generates' periodic wave packets whose amplitude is proportional to the initial value u_{ey_0}. At small initial values the amplification

https://doi.org/10.1017/S0022377803002319 Published online by Cambridge University Press

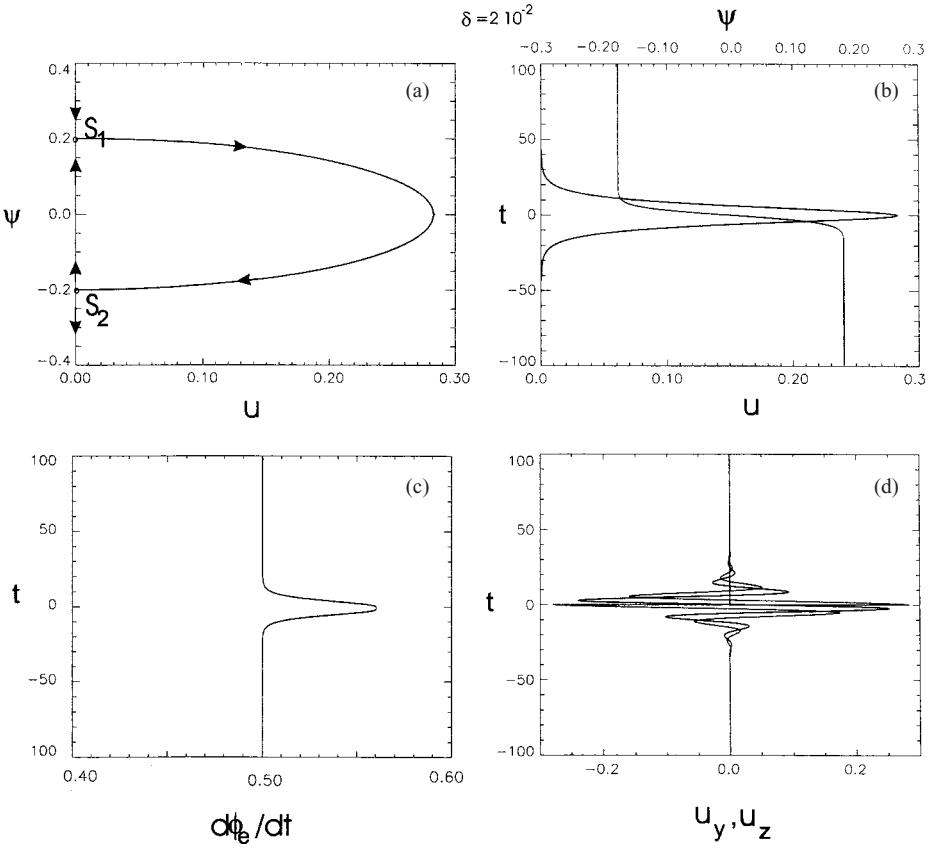

Figure 3. The same as in Fig. 2 but for solitons with higher speeds ($M_A = 0.51$).

reaches a factor of ∼25. The width of the wave packets decreases with increasing u_{ey_0}, although the wavelength of the embedded small-scale oscillations remains practically constant.

Although the fixed point at $\psi = 0$ disappears for $\delta < 0$, free phase orbits similar to the orbits shown in Fig. 1(b) remain and associated with these are solutions in the form of wave packets. The amplitude of these wave packets is also determined by initial conditions, and decreases with $|\delta|$ (38b). Figure 6 shows the solutions of numerical integration of (19) and (20) for several values of $M_A \leqslant 1/2$ for a given 'initial' perturbation of the system ($u_{ey_0} = 0.01$). A decrease of M_A brings about decreases in the width and amplitude of the wave packets.

3.2. Approximation of arbitrary phases ψ and small amplitudes

We now consider the exact nonlinear equations (29) and (30) with arbitrary phase ϕ using the expansion of (31) ($u_x \approx 1 - u_e^2/2\mu$). Introducing new normalized variables $\varphi = 2M_A \cos(\phi/2)$, $u = u_e/\sqrt{2\mu}$ and $t = M_A x$ leads to the following system of coupled differential equations:

$$\frac{du}{dt} = \varphi u \sin\frac{\phi}{2}, \tag{48a}$$

https://doi.org/10.1017/S0022377803002319 Published online by Cambridge University Press

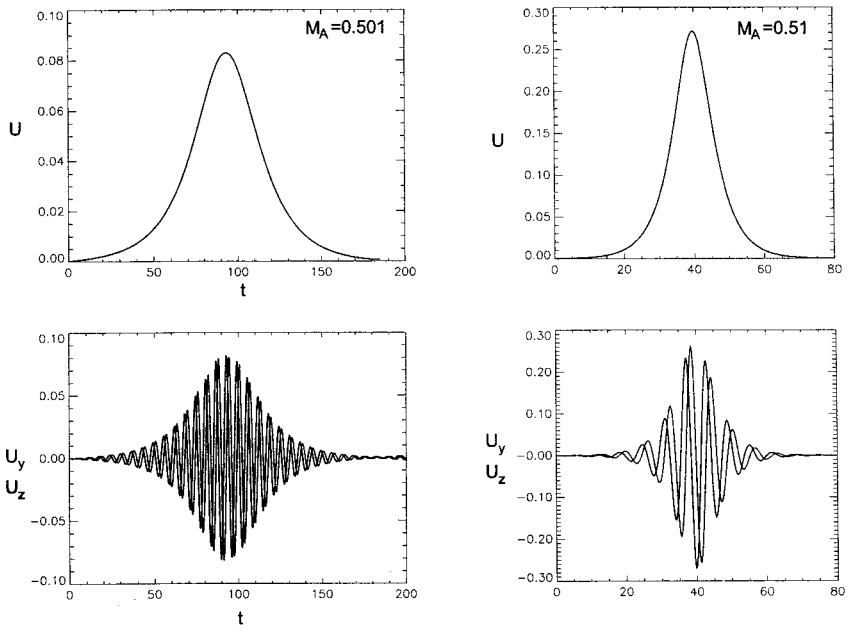

Figure 4. Examples of oscillitons with $M_{\rm A} = 0.501$ and $M_{\rm A} = 0.51$. Solid and dashed curves on the bottom panel show respectively u_y and u_z.

$$\frac{d\varphi}{dt} = (1 + u^2 - \varphi^2) \sin\frac{\phi}{2}. \tag{48b}$$

Note that the phase portrait of this system coincides with the phase portrait of the reduced equations,

$$\frac{du}{dt} = \varphi u, \tag{49a}$$

$$\frac{d\varphi}{dt} = (1 + u^2 - \varphi^2), \tag{49b}$$

if $\sin(\phi/2) \neq 0$ ($\phi \neq 0, \pm 2n\pi$) (recall that the approximation of small phases $\phi \ll 1$ was investigated in the preceding section). Equations (48), and correspondingly (49), also possess the integral

$$G = \tfrac{1}{2}u^2(1 + u^2/2 - \varphi^2) \tag{50}$$

so that

$$\varphi = \pm\sqrt{1 + \frac{u^2}{2} - \frac{2C_2}{u^2}} \tag{51}$$

and

$$\frac{du}{dt} = \pm\frac{u}{2M_{\rm A}}\sqrt{\left(1 + \frac{u^2}{2} - \frac{2C_2}{u^2}\right)\left[(4M_{\rm A}^2 - 1) - \frac{u^2}{2} + \frac{2C_2}{u^2}\right]}, \tag{52}$$

where C_2 is a constant. Soliton solutions correspond to $C_2 = 0$. Putting $M_{\rm A} = 1/2(1+\delta)$ and assuming that $\delta \ll 1$, $u^2 \ll 2$, gives (38b) in the small phase approximation. The amplitude of the soliton, determined only by the expression in the

https://doi.org/10.1017/S0022377803002319 Published online by Cambridge University Press

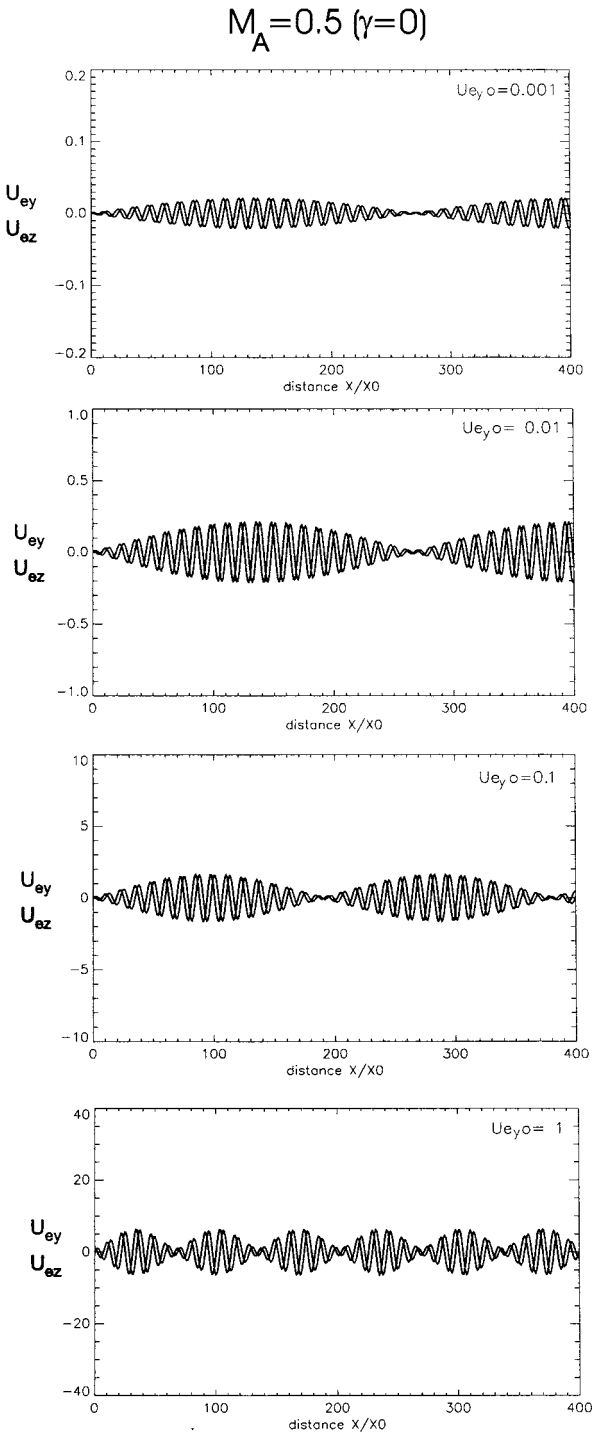

Figure 5. Examples of a sequence of wave packets corresponding to the phase trajectories shown in Fig. 1(b). The amplitude of wave packets is determined by the value of an 'initial' perturbation. Solid and dashed curves show u_y and u_z.

https://doi.org/10.1017/S0022377803002319 Published online by Cambridge University Press

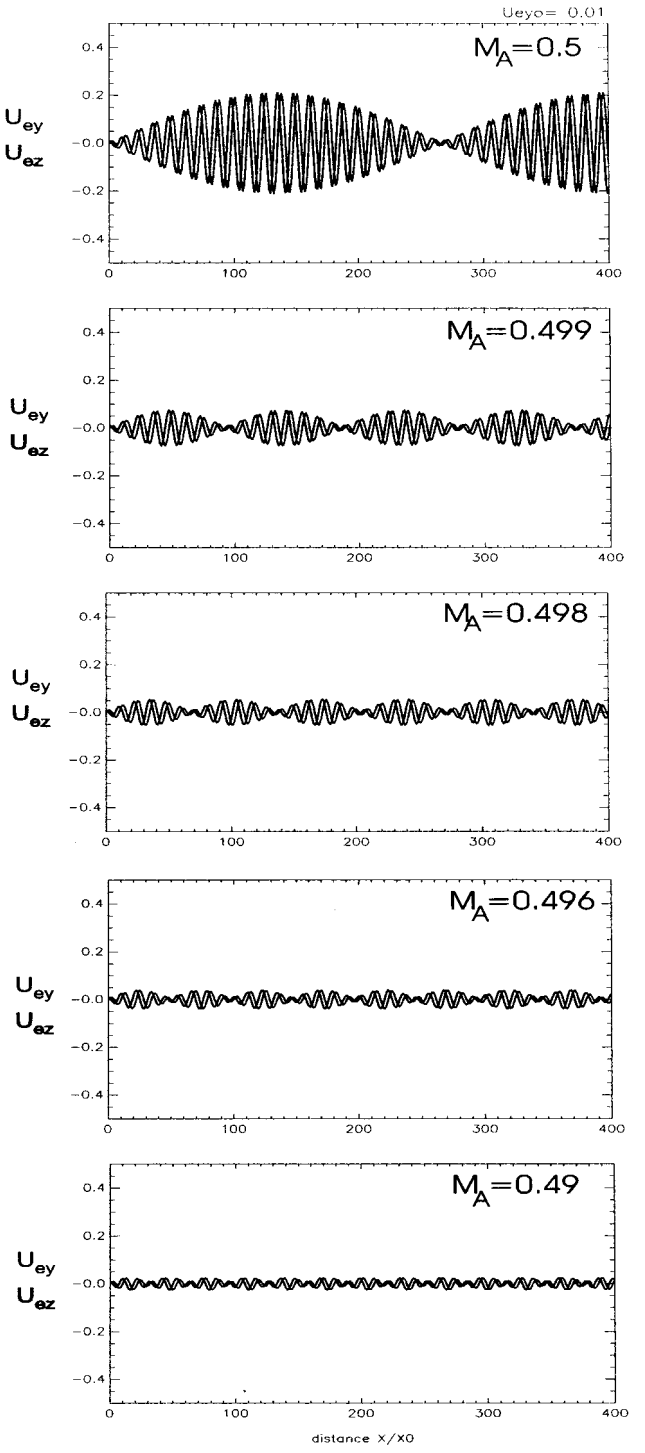

Figure 6. Wave packets generated at $M_{\rm A} \leqslant 1/2$ by the initial perturbation $u_{ey_0} = 0.01$ of the system. Solid and dashed curves show respectively u_y and u_z.

https://doi.org/10.1017/S0022377803002319 Published online by Cambridge University Press

square brackets of (52), remains the same as in the approximation of small phases,

$$u_{\max} = \sqrt{2}\,\mathscr{M}_{\rm A}. \tag{53}$$

Integration of (52) gives the analytical solution,

$$\sqrt{\mathscr{M}_{\rm A}^2+1}\,\ln\frac{2\alpha+\beta u^2+2\sqrt{\alpha P}}{2\big(\mathscr{M}_{\rm A}^2+1\big)u^2} = \pm t. \tag{54}$$

Here $\mathscr{M}_{\rm A}^2 = 4M_{\rm A}^2 - 1$, $\alpha = 4\mathscr{M}_{\rm A}^2$, $\beta = 2(\mathscr{M}_{\rm A}^2 - 1)$, $P = \alpha + \beta u^2 - u^4$, and the constant of integration is determined from $u = u_{\max} = \sqrt{2}\,\mathscr{M}_{\rm A}$.

Figure 7 presents the characteristics of a solution with $M_{\rm A} = 0.6$. The orbit corresponding to the soliton is shown by the thick curve in the coordinates $(u, \psi = \phi M_{\rm A})$, where $\phi = 2\arccos(\varphi/2M_{\rm A})$ (Fig. 7(a)). The solid curves depict periodic orbits. It is observed that the picture remains qualitatively the same, with two saddle points connected by a 'soliton trajectory' and an O-point, but the amplitude of the soliton reaches large values for which the approximation ($u_{\rm e} \ll \sqrt{\mu}$) is no longer strictly valid. The solid curves in Figs 7(b,c) show the solutions of the exact equations, the heteroclinic orbit ('soliton trajectory') of (34) and the soliton structure found from numerical integration of (29) and (30) with $M_{\rm A} = 0.6$. The dashed curves present the results of the approximation used. Despite the qualitative similarity a significant difference is revealed in the amplitudes. Note that in the approximation solutions, $u^2 \ll \mu$, the factor $1/2$ appears in the expansion of (31) and this leads to larger soliton amplitudes than in fact the exact equations would allow as we show subsequently. Figure 7(d) depicts how the phases $\psi, \phi_{\rm e}, \phi_{\rm p}$ vary with the distance t. Far from the soliton core the slopes of the curves $\phi_{\rm e,p}(t)$ are constant ($d\phi_{\rm e,p}/dt = 0.5$), i.e. the oscilliton contains 'material' proportional to $\sim\cos(0.5t)$ or $\sin(0.5t)$. Within the first portion of the core the phases $\phi_{\rm e}, \phi_{\rm p}$ grow faster than at small t but, after the centre of the soliton, $d\phi_{\rm e,p}/dt$ decreases once more approaching the value $1/2$. It is important to note that the phases $\phi_{\rm e}$ and $\phi_{\rm p}$ are always different, thereby ensuring the existence of nonlinear stationary solutions with $u \neq$ const. At large amplitudes the wavelength of the embedded oscillations becomes comparable with the soliton width and the oscilliton begins to resemble a classical soliton with a rather complicated core (Fig. 8).

Although the exact equations (29) and (30) are more complicated, we can evaluate the amplitude of a soliton as a function of the Mach number. Expanding expression (33) for small phases and comparing with (38a) yields a constant $C = \mu/M_{\rm A}^2$ for solitons ($C_1 = 0$). At the centre of a soliton $du_{\rm e}/dx = 0$, which leads to

$$u_{\rm emax} = \frac{\sqrt{\mu}}{2M_{\rm A}^2}\sqrt{4M_{\rm A}^2 - 1}\,, \tag{55}$$

or in the variables u and $\mathscr{M}_{\rm A}$,

$$u_{\max} = \sqrt{2}\,\frac{\mathscr{M}_{\rm A}}{\mathscr{M}_{\rm A}^2+1}. \tag{56}$$

This differs from the expression (53) by the factor $1/(\mathscr{M}_{\rm A}^2+1)$. It is evident that the critical Mach number, above which smooth oscillitons cannot be constructed, corresponds to $u_x \to 0$ which occurs at $u = 1/\sqrt{2}$, i.e. $\mathscr{M}_{\rm Acrit} = 1$, or $M_{\rm Acrit} = 1/\sqrt{2} \approx 0.7$.

https://doi.org/10.1017/S0022377803002319 Published online by Cambridge University Press

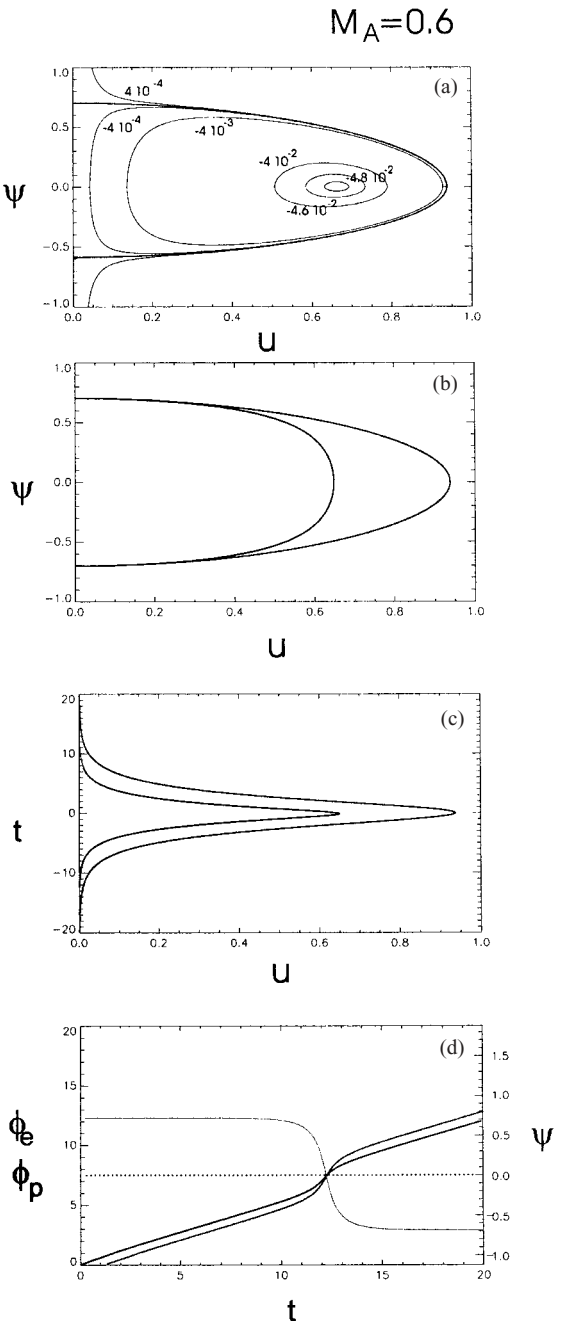

Figure 7. (a) The phase portrait of the system at $M_{\rm A} = 0.6$ in the approximation of small amplitudes. The thick curve corresponds to the soliton trajectory. (b) The soliton trajectories in the approximation of small amplitudes (the dashed curve) and from the exact equations (the solid curves). (c) Comparison of the soliton solutions in both cases. (d) Variations of the phases $\psi, \phi_{\rm e}, \phi_{\rm p}$ with the distance t.

https://doi.org/10.1017/S0022377803002319 Published online by Cambridge University Press

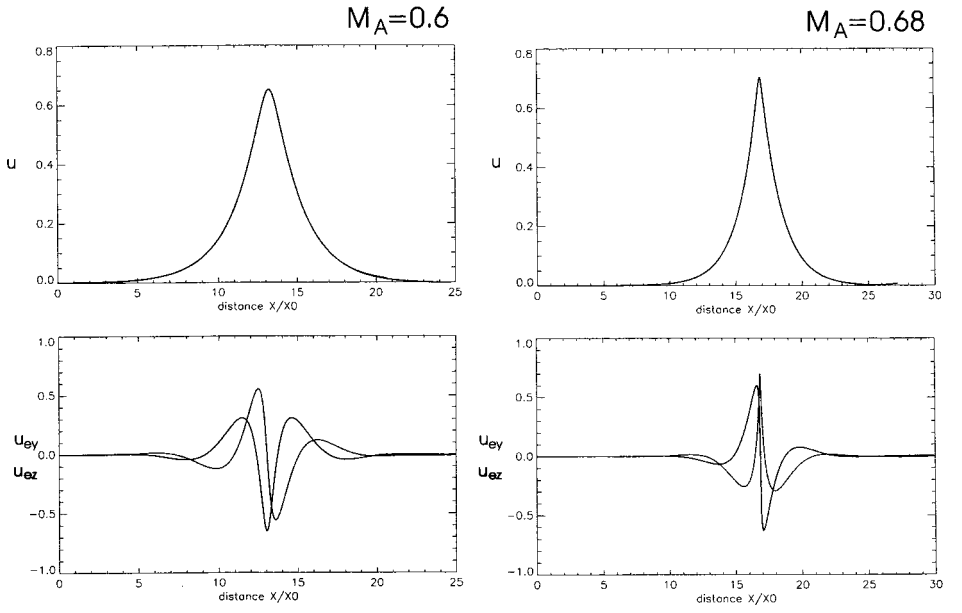

Figure 8. Oscillitons with large amplitudes. Top panel shows the amplitude of the transverse velocity of the electrons. Solid and dashed curves on the bottom panels show respectively u_{ey} and u_{ez}.

4. Nonlinear stationary waves propagating obliquely to the magnetic field

Here we consider stationary waves propagating in the x-direction so that in this frame the plasma appears to flow obliquely to the magnetic field $\mathbf{B}$ ($\mathbf{B} = B_x, 0, B_{z0}$). Faraday's law requires that the electric field transverse to the flow is constant, and hence $E_y = u_0 B_{z0}, E_z = 0$. The fully nonlinear system of equations (26) for the transverse velocities of the electrons and protons in the case of oblique propagation now becomes

$$\frac{dv_{e\pm}}{dt} = \mp i\left[M_\parallel^2(v_{e\pm} + \mu v_{p\pm}) - v_{e\pm}/u_x\right] + \sin\theta\left(1 - \frac{1}{u_x}\right), \tag{57a}$$

$$\mu\frac{dv_{p\pm}}{dt} = \pm i\left[M_\parallel^2(v_{e\pm} + \mu v_{p\pm}) - v_{p\pm}/u_x\right] - \sin\theta\left(1 - \frac{1}{u_x}\right), \tag{57b}$$

where $v_{e\pm}/\cos\theta = u_{ey} \pm i u_{ez}$, $v_{p\pm}/\cos\theta = u_{py} \pm i u_{pz}$, $t = x\cos\theta$, $M_\parallel = M_A/\cos\theta$, and the magnetic field $(\cos\theta, 0, \sin\theta)$ is expressed via the transverse velocities by using the momentum flux constants, $\mu v_{p\pm} + v_{e\pm} = b_\pm/M_\parallel^2$. Here $b_\pm = B_y \pm i b_z$ ($b_z = B_z - \sin\theta$). Energy flux conservation,

$$(\mu+1)\left(u_x^2 - 1\right) + \mu\left(u_{py}^2 + u_{pz}^2\right) + u_{ey}^2 + u_{ez}^2 + \frac{2E_y(B_z - \sin\theta)}{M_A^2} = 0, \tag{58}$$

yields

$$u_x = \frac{1}{\sqrt{\mu}\cos\theta}\left(\mu\cos^2\theta - v_e^2 - \mu v_p^2 - 2\sin\theta b_z/M_\parallel^2\right)^{1/2}, \tag{59}$$

https://doi.org/10.1017/S0022377803002319 Published online by Cambridge University Press

where $v_{\mathrm{e,p}} = (v_{\mathrm{e,p}y}^2 + v_{\mathrm{e,p}z}^2)^{1/2}$. It now follows that

$$\frac{d}{dt}\left(\mu^2 v_{\mathrm{p}}^2 - v_{\mathrm{e}}^2\right) = 2\sin\theta\left(\frac{1}{u_x} - 1\right) B_y/M_{\parallel}^2, \tag{60}$$

thus instead of the parallel result (28) $\mu v_{\mathrm{p}} \neq v_{\mathrm{e}}$ and we may expect the appearance of smaller-scale oscillations superimposed on the large-scale variations in v_{e} and v_{p} associated with the terms proportional to B_y and b_z.

In the general case of obliquely propagating waves, the four coupled differential equations (57a–b), which totally describe the nonlinear dynamics, cannot be reduced to two equations as was done previously in the case of parallel propagation. However, some important features of stationary solutions can be found in the approximation of small amplitudes. In terms of the amplitudes and phases of the transverse motion of the electrons and protons the system may be written in the form

$$\frac{dv_{\mathrm{e}}}{dt} = M_{\parallel}^2 \mu v_{\mathrm{p}} \sin\phi + \sin\theta\left(1 - \frac{1}{u_x}\right)\cos\phi_{\mathrm{e}}, \tag{61a}$$

$$\mu\frac{dv_{\mathrm{p}}}{dt} = M_{\parallel}^2 v_{\mathrm{e}} \sin\phi - \sin\theta\left(1 - \frac{1}{u_x}\right)\cos\phi_{\mathrm{p}}, \tag{61b}$$

$$\frac{d\phi_{\mathrm{e}}}{dt} = -M_{\parallel}^2\left(1 + \frac{\mu v_{\mathrm{p}}}{v_{\mathrm{e}}}\cos\phi\right) + \frac{1}{u_x} - \frac{\sin\theta}{v_{\mathrm{e}}}\left(1 - \frac{1}{u_x}\right)\sin\phi_{\mathrm{e}}, \tag{61c}$$

$$\frac{d\phi_{\mathrm{p}}}{dt} = M_{\parallel}^2\left(1 + \frac{v_{\mathrm{e}}}{\mu v_{\mathrm{p}}}\cos\phi\right) - \frac{1}{\mu u_x} + \frac{\sin\theta}{\mu v_{\mathrm{p}}}\left(1 - \frac{1}{u_x}\right)\sin\phi_{\mathrm{p}}, \tag{61d}$$

where we have used $v_{\mathrm{p,e},\pm} = v_{\mathrm{p,e}} e^{\pm i\phi_{\mathrm{p,e}}}$ and $\phi = \phi_{\mathrm{p}} - \phi_{\mathrm{e}}$. The equation for the phase ϕ may be written as

$$\frac{d\phi}{dt} = 2M_{\parallel}^2 + M_{\parallel}^2\left(\frac{\mu v_{\mathrm{p}}}{v_{\mathrm{e}}} + \frac{v_{\mathrm{e}}}{\mu v_{\mathrm{p}}}\right)\cos\phi - \frac{1}{u_x} + \sin\theta\left(1 - \frac{1}{u_x}\right)\left(\frac{\sin\phi_{\mathrm{e}}}{v_{\mathrm{e}}} + \frac{\sin\phi_{\mathrm{p}}}{\mu v_{\mathrm{p}}}\right). \tag{62}$$

It is reasonable to assume that at least for small-amplitude nonlinear waves ($u_x \sim 1$): $\mu v_{\mathrm{p}} \approx v_{\mathrm{e}}$, $(\phi_{\mathrm{e}} + \phi_{\mathrm{p}})/2 \sim \bar{\phi}_{\mathrm{e}}$ and $d\bar{\phi}_{\mathrm{e}}/dt \sim M_{\parallel\mathrm{thres}}$, where $M_{\parallel\mathrm{thres}}$ is the threshold value of the Mach number in excess of which stationary solutions exist (for $\theta = 0$, $M_{\parallel\mathrm{thres}} = 1/2$). These assumptions are justified *a posteriori* by numerically solving the exact system of differential equations. Then in the approximation of small amplitudes and phases ϕ, the system again reduces to two coupled differential equations for the amplitude v_{e} ($\approx \mu v_{\mathrm{p}}$) and the phase ϕ:

$$\frac{dv_{\mathrm{e}}}{dt} = M_{\parallel}^2 v_{\mathrm{e}}\phi - \frac{v_{\mathrm{e}}^2 \sin\theta\cos\bar{\phi}_{\mathrm{e}}}{2\mu\cos^2\theta} - \frac{\sin^2\theta}{\mu\cos^2\theta} v_{\mathrm{e}} \sin 2\bar{\phi}_{\mathrm{e}}, \tag{63a}$$

$$\frac{d\phi}{dt} = 4M_{\parallel}^2 - 1 - \frac{4\sin^2\theta\sin^2\bar{\phi}_{\mathrm{e}}}{\mu\cos^2\theta} - \frac{v_{\mathrm{e}}^2}{2\mu\cos^2\theta} - M_{\parallel}^2\phi^2 - \frac{3v_{\mathrm{e}}\sin\theta}{\mu\cos^2\theta}\sin\bar{\phi}_{\mathrm{e}}, \tag{63b}$$

in which we have used the expansion

$$\frac{1}{u_x} \approx 1 + \frac{v_{\mathrm{e}}^2}{2\mu\cos^2\theta} + \frac{2v_{\mathrm{e}}\sin\theta}{\mu\cos^2\theta}\sin\bar{\phi}_{\mathrm{e}}, \tag{64}$$

which is valid for $v_{\mathrm{e}} \ll \sqrt{\mu}\cos\theta$.

https://doi.org/10.1017/S0022377803002319 Published online by Cambridge University Press

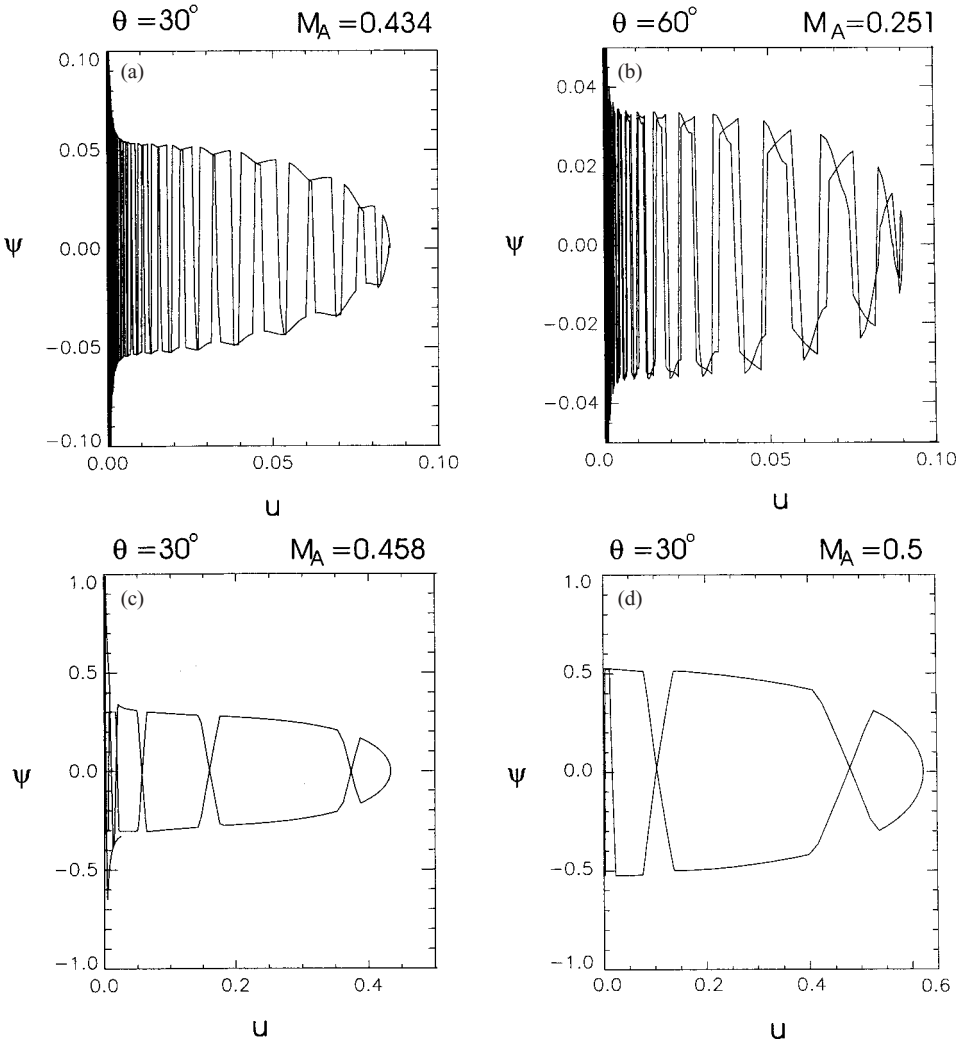

Figure 9. Phase portraits found by solving the exact equations for stationary waves propagating obliquely to the magnetic field (the solutions are very close to oscilliton type of solutions).

In rescaled form ($u^2 = v_e^2/2\mu\cos^2\theta, \psi = M_\parallel\phi, t' = M_\parallel t$) the system (63) is

$$\frac{du}{dt'} = u\psi - \frac{u^2}{M_A}\frac{\sin\theta\cos\bar{\phi}_e}{\sqrt{2\mu}} - \frac{u\sin^2\theta\sin 2\bar{\phi}_e}{M_A\mu\cos\theta}, \tag{65a}$$

$$\frac{d\psi}{dt'} = 4M_\parallel^2 - 1 - \frac{4\sin^2\theta\sin^2\bar{\phi}_e}{\mu\cos^2\theta} - u^2 - \psi^2 - 3\sqrt{\frac{2}{\mu}}u\frac{\sin\theta}{\cos\theta}\sin\bar{\phi}_e. \tag{65b}$$

In the absence of the last two terms in (65a) and the last term in (65b) this system coincides with the system (36) (for waves propagating parallel to the magnetic field)

https://doi.org/10.1017/S0022377803002319 Published online by Cambridge University Press

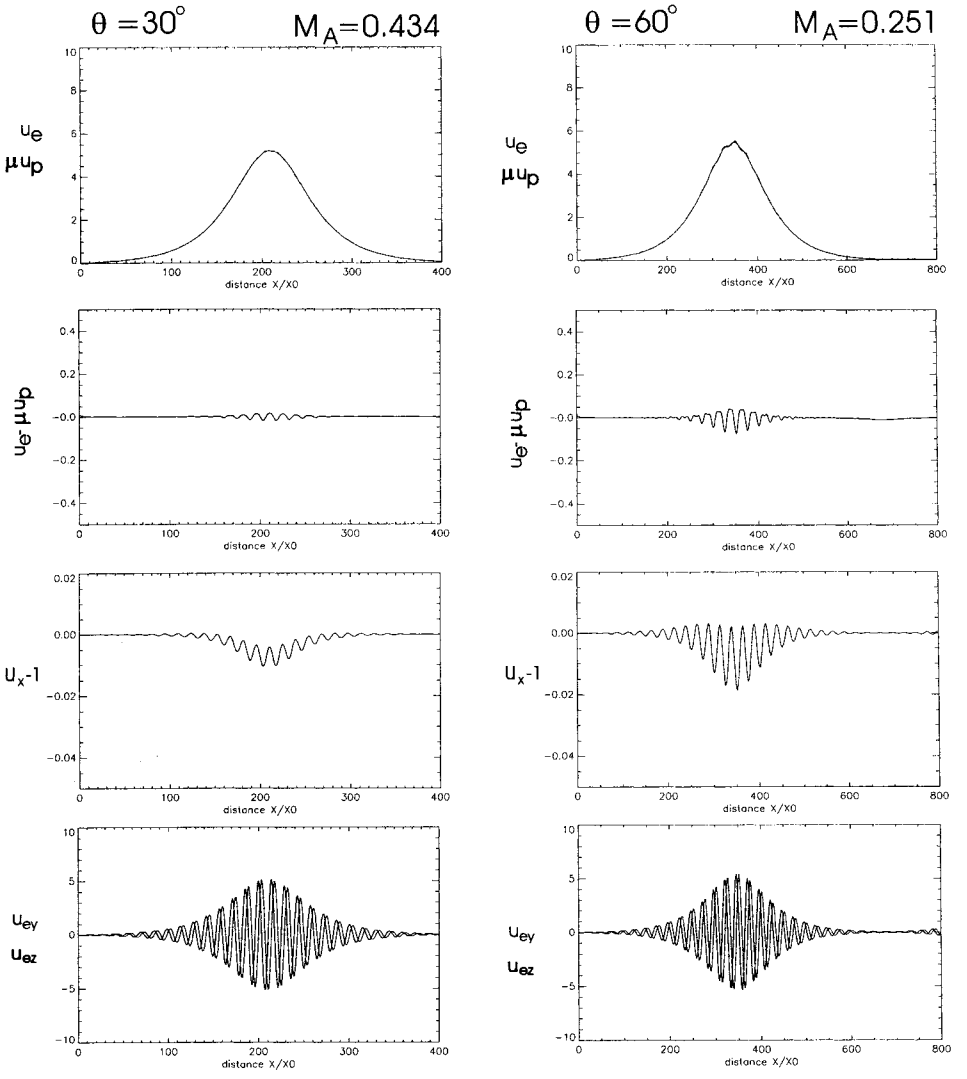

Figure 10. The structure of obliquely propagating whistler oscillitons. From the top to the bottom are shown the transverse amplitudes of the electron (solid curves) and proton (dashed curves) speeds, the difference between $u_{\rm e}$ and $\mu u_{\rm p}$, variations in the longitudinal component of the velocity and the u_{ey} and $u_{\rm ez}$ components of the electron speed.

which admits oscilliton type solutions if

$$4M_{\parallel}^2 - 1 - \frac{4\sin^2\theta\sin^2\bar{\phi}_{\rm e}}{\mu\cos^2\theta} > 0$$

or solutions in the form of periodic wave packets if

$$4M_{\parallel}^2 - 1 - \frac{4\sin^2\theta\sin^2\bar{\phi}_{\rm e}}{\mu\cos^2\theta} = 0.$$

For $\tan\theta \ll \sqrt{\mu}/2$ the threshold value of the Mach number is $M_{\parallel\rm thres} = 1/2$ or $M_{\rm Athres} = \cos\theta/2$. The terms, which we neglect for the moment, contain a 'periodic

https://doi.org/10.1017/S0022377803002319 Published online by Cambridge University Press

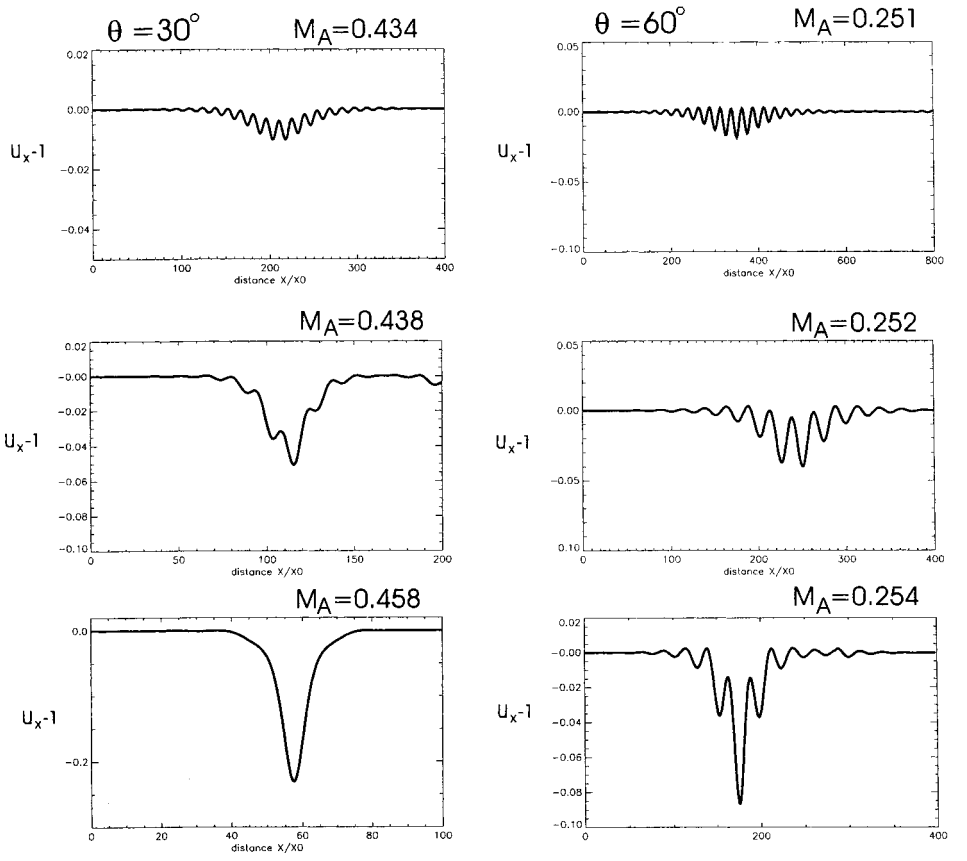

Figure 11. Obliquely propagating oscillitons with different amplitudes.

part' proportional to the sine or cosine of $\bar{\phi}_e$ ($\bar{\phi}_e \sim M_\parallel t'$) that essentially modifies the dynamics of the system (in a certain sense they can be considered as the 'forcing terms' for the system (36)). Figures 9(a,b) show the phase portraits corresponding to the solutions which are very close to soliton-type solutions with $\theta = 30°(60°)$ and $M_\parallel = M_{\parallel \mathrm{thres}} + 0.001$ (the results of numerically solving the exact equations). Although two saddle points at $u = 0, \psi = \pm\sqrt{4M_\parallel^2 - 1}$ remain, a new important feature appears, namely the heteroclinic orbit undergoes 'sinusoidal' variations with a periodic change in the sign of the phase ψ. However such 'heteroclinic tangle' is not a signature of transition to chaos. Since the nonlinear system cannot be reduced to two differential equations and is described by four variables one may expect regular trajectories in four-dimensional space. Figure 10 presents the results of numerically solving the exact nonlinear equations (57) for oscillitons propagating obliquely to the magnetic field. The amplitudes $v_e = u_e \cos\theta$ and $\mu v_p = \mu u_p \cos\theta$ (the top panels) are almost the same although the appearance of small ripples on the curves $u_e(\mu u_p)$ is observed. The longitudinal component of the velocity u_x clearly reveals oscillating behavior superimposed on a soliton-like structure. Figure 11 depicts how u_x varies with increasing Alfvén Mach number. The width of an oscilliton decreases and its core contains a smaller number of oscillations. This feature is also clearly observed in the phase portraits at high Mach numbers (Figs 9(c,d)).

https://doi.org/10.1017/S0022377803002319 Published online by Cambridge University Press

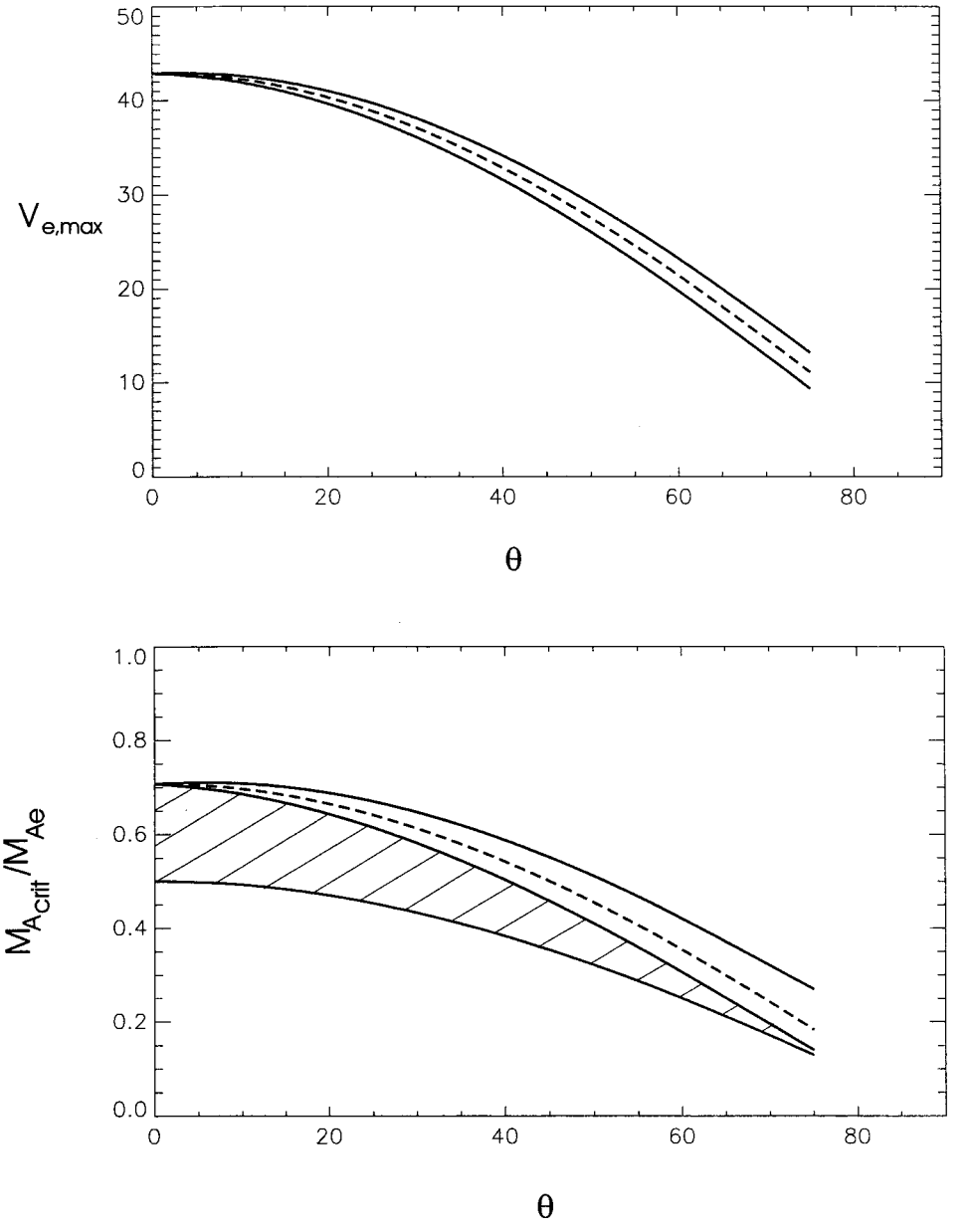

Figure 12. (a) The dependence of the maximum electron speed v_{emax} which can be achieved in the whistler oscillitons on the obliqueness θ for $\sin\bar{\phi}_{\mathrm{e}} = 0, \pm 1$ (the dashed and solid curves). (b) The corresponding critical Alfvén Mach numbers. The dotted curve shows the threshold value of the Mach number.

The maximum speed of the electrons in oscillitons can be estimated from the condition $u_x \to 0$,

$$v_{\mathrm{emax}} = -2\sin\theta\sin\bar{\phi}_{\mathrm{e}} \pm \sqrt{4\sin^2\theta\sin^2\bar{\phi}_{\mathrm{e}} + \mu\cos^2\theta}, \tag{66}$$

https://doi.org/10.1017/S0022377803002319 Published online by Cambridge University Press

where $\bar{\phi}_e \approx \cos(\theta t/2)$. It will be observed that this amplitude is now a weak function of t. Figure 12(a) shows the range of v_{emax} as a function of the obliqueness θ for $\sin\bar{\phi}_e = 0, \pm 1$ (the dashed and solid curves). The corresponding critical Mach numbers can be estimated by generalizing the parallel case as

$$\mathscr{M}_{\parallel cr} = \frac{1+\sqrt{1-4v_{emax}^2}}{2} \quad \text{or} \quad M_{Acr} = \frac{\cos\theta}{2}\sqrt{1+\mathscr{M}_{\parallel cr}^2}. \tag{67}$$

Figure 12(b) shows the threshold value of the Alfvén Mach number in excess of which stationary solutions exist (the dotted curve), and the critical Mach numbers above which the 'overturning' of waves occurs (the black solid and dashed curves). Smooth solutions exist in the shaded area between these curves.

5. Summary and conclusions

We have developed a fully nonlinear theory for whistler solitons and periodic waves propagating parallel to the magnetic field. The treatment involves the exact solutions of the coupled nonlinear differential equations in which the electron and proton dynamics are placed on an equal footing. By making use of the constants of motion, the momentum and energy fluxes, it is shown that in stationary whistlers the transverse amplitude of the electron speed $|u_e| = (u_{ey}^2 + u_{ez}^2)^{1/2}$ is equal to the proton transverse speed $|u_p|$ multiplied by the mass ratio factor $\mu = m_p/m_e$. This implies that the transverse momentum carried by the electrons and protons in the wave frame are equal, $\mu u_p = u_e$, and explicitly shows that the momentum fluxes of both species are required to balance the wave magnetic stresses. Moreover, the phases of the electron (ϕ_e) and proton (ϕ_p) motions are different and the system is analogous to two nonlinearly coupled pendula with different periods. This vitally important feature of the nonlinear equations distinguishes the nonlinear system from the linear one, where in the latter the dispersion equation for stationary waves does not contain the proton mass. However, the linear dispersion equation does provide us with the necessary condition for the existence of nonlinear stationary waves, namely that the electron Alfvén Mach number must exceed the critical value, $M_{Ae} > 1/2$. Another interesting feature which follows already from the linear dispersion equation is that the wave number is complex in the parameter range where stationary nonlinear waves exist. This means that evanescent type solutions also contain an oscillatory core.

The full system of nonlinear equations can be reduced to two coupled differential equations, which describe the transverse wave motion, for the amplitude u_e and the phase $\phi = \phi_p - \phi_e$. Neglect of the proton contribution yields only trivial solutions with $u_e = \text{const}$. It is interesting to note that if the protons are included but not in a completely self-consistent manner, for example by using the relation between the proton and electron transverse speeds from the linear theory, the phase $\phi = 0$ and still only the trivial solution $u_e = \text{const}$, results.

The system of nonlinear differential equations for the amplitude u_e and the phase ϕ completely describe the dynamics of the electrons and protons. This system possesses a phase-portrait integral which is constant along the solution trajectories and enables us to deduce the main features of the dynamics. There is a family of periodic orbits around an O-type point limited by a heteroclinic orbit connecting two saddle points, with a family of free orbits outside. In a certain sense, the system

https://doi.org/10.1017/S0022377803002319 Published online by Cambridge University Press

is similar to a nonlinear pendulum (in our case, two nonlinear pendula, one for the electrons and another one for the protons coupled via the phase $\phi = \phi_p - \phi_e$).

We have analysed in some detail the approximation of 'small' amplitudes ($u_e \ll \sqrt{\mu}$, where the speeds are normalized to the electron Alfvén speed) and small (and also arbitrary) phases. In this case we find exact solutions in terms of elliptic integrals of the first kind. For the soliton type solutions which correspond to a heteroclinic orbit connecting two saddle points, analytical solutions for the amplitude and phases ϕ_e, ϕ_p and ϕ are also found. These phases provide us with structures which differ from classical solitons by the existence of an oscillating core and therefore are called oscillitons. The remarkable feature is that the wave number of the embedded oscillations is very close to the wave number at which the phase velocity for whistlers has a maximum (note that a wave number k is normalized to Ω_e/u_0, i.e. the wave number of the oscillations is Ω_e/V_{Ae}). The relation between the amplitude of the envelope of such an oscilliton and its Alfvén Mach number is similar to the classical soliton. There is a critical Alfvén Mach number ($M_{Acrit} = 1/\sqrt{2}$) above which smooth oscilliton solutions cannot be constructed and this corresponds to where the longitudinal speed of the electrons and protons go to zero ($u_e \to \sqrt{\mu}$).

The existence of the O-type fixed point at $u = ((1 - 1/16M_A^4)/2)^{1/2}$ would admit the construction of a weak dispersive whistler shock by including a small amount of dissipation. After several soliton-like pulses the system would go to a new equilibrium point. Such a shock would be characterized by a sequence of whistler packets of different widths.

Another interesting class of solutions which may have many applications occurs at $M_{Ae} = 1/2$. In this case, two saddle points degenerate to one and the system can 'generate' a periodical sequence of wave packets. The small-scale oscillations in these packets are determined by the phases ϕ_e or ϕ_p. The nonlinear beating between both modes gives a stationary wave packet where the amplitude of the envelope is varying and the wavelength is determined by the phase $\phi = \phi_e - \phi_p$. The amplitude of these structures is also sensitive to the 'initial' perturbation of the system. The fact that wave packets of nonlinear stationary whistlers appear just at the border ($M_{Ae} = 1/2$) (in the space $\omega/k - k$), where the usual propagating modes (with real k) also exist, means that these structures can be effectively seeded by any mechanism of whistler generation. For example, cyclotron resonance instability fed by a temperature anisotropy can excite a rather broad spectrum of emissions via the anomalous Doppler resonance. The modes with the phase (group) speed equal to $M_{Ae} = 1/2$ are selected and amplified from this wave ensemble since the electrons and the protons interplay effectively and the nonlinear system begins to 'resonate' giving rise to wave packets with an oscillating content at $f_{ce}/2$. This mechanism may be responsible for the generation of the 'lion roars' observed in the Earth's magnetosheath (Sauer et al. 2002b).

For stationary waves propagating obliquely to the magnetic field, oscillitons and periodic wave packets also exist, although the system becomes more complicated, now being described by four coupled differential equations for the amplitudes and phases of the transverse motion of the electrons and protons. The threshold Alfvén Mach number in excess of which oscillitons can be constructed now becomes $\cos\theta/2$. The wave number of the embedded small-scale oscillations is also close to the wave number at which the dispersive curve (ω/k–k) for obliquely propagating whistlers has a maximum (at $k_r \sim \cos\theta/2$ or, in the original coordinates, at $k = \Omega_e/V_{Ae}$, i.e. it does not depend on the angle θ). Interestingly that at large propagation angles

https://doi.org/10.1017/S0022377803002319 Published online by Cambridge University Press

the oscilliton speed occurs in the range of values common to the solar wind and therefore one may expect the appearance of oscilliton substructures embedded in a weak (dispersive) oblique bow shock structure.

Acknowledgements

ED thanks the Deutsche Forschungsgemeinschaft and the Max-Planck-Gesellschaft for supporting this work by grants. The work was also supported by an INTAS-ESA-99-00066 grant.

References

Dubinin, E., Sauer, K. and McKenzie, J. F. 2002 Solitons and oscillitons in cold bi-ion plasmas: A parameter study. *J. Plasma Phys.* **68**, 27.

Montgomery, D. C. 1959 *Phys. Fluids* **2**, 585.

Kakutani, T. 1966 *J. Phys. Soc. Japan* **23**, 385.

Sauer, K., Dubinin, E. and McKenzie, J. F. 2001 New type of soliton in bi-ion plasmas and possible implications. *Geophys. Rev. Lett.* **28**, 3589.

Sauer, K., Dubinin, E. and McKenzie, J. F. 2002a Coherent waves in multi-ion plasmas. *Physica Scripta* T **98**, 52.

Sauer, K., Dubinin, E. and McKenzie, J. F. 2002b Coherent wave emissions by whistler oscillitons: application to lion roars. *Geophys. Res. Lett.* **29**, 24, 79, 2002.

Stix, T. 1992 *Waves in Plasmas*. New York: American Institute of Physics.